Reliability Engineering and System Safety 272 (2026) 112582

Contents lists available at ScienceDirect

Reliability Engineering and System Safety

journal homepage: www.elsevier.com/locate/ress

Predicting seismic floor response for nuclear power plant structures with time-series uncertainty propagation using attention-enhanced multimodal deep learning

Jingoo Lee [a], Seungjun Lee [b], Young-Joo Lee [a,*], Jaebeom Lee [b,c,**]

[a] Department of Civil, Urban, Earth, and Environmental Engineering, Ulsan National Institute of Science and Technology (UNIST), Ulsan 44919, Republic of Korea
[b] Division of Physical Metrology, Korea Research Institute of Standards and Science, 267 Gajeong-ro, Yuseong-gu, Daejeon 34113, Republic of Korea
[c] Precision Measurement Major, University of Science and Technology, 217 Gajeong-ro, Yuseong-gu, Daejeon 34113, Republic of Korea

ARTICLE INFO

Keywords:
Seismic response prediction
Nuclear power plants
Multimodal deep learning
Uncertainty quantification

ABSTRACT

Ensuring the safety and reliability of critical equipment in nuclear power plants (NPPs) requires accounting for uncertainties in structural parameters. However, probabilistic methods based on finite element analysis (FEA) can be computationally expensive and impractical for real-time safety assessment. In this study, we propose a surrogate framework based on deep learning that directly generates full time-history acceleration responses at multiple structural locations to reduce the computational cost of probabilistic analysis by replacing FEA. The architecture is organized into two encoders, including a *structural parameter encoder* and a *seismic encoder* enabling feature extraction from two distinct input modalities. Their latent representations are fused and mapped using a *response decoder* that reconstructs multi-output acceleration responses. The results of experimental validation show that the model achieved an average maximum mean absolute percentage error (mMAPE) of 1.37 %. Beyond deterministic surrogate predictions, the proposed framework generates probabilistic responses to capture the variability of structural response over time and instantly estimate exceedance probabilities with respect to equipment-level thresholds. This probabilistic inspection capability extends conventional deterministic safety checks to a reliability-informed paradigm to offer a computationally efficient solution for the assessment of important equipment in NPPs.

1. Introduction

Nuclear power plants (NPPs) contain critical equipment that is highly susceptible to seismically induced vibrations. Such vibration-induced failures can lead to plant shutdown even when the ground motion (GM) remains within the linear-elastic response range of primary structural components. Historical earthquake events demonstrate this vulnerability. For example, the 2016 Gyeongju earthquake (with a peak ground acceleration (PGA 0.12 g), the 2011 North Anna earthquake (PGA 0.26 g), and the 2019 Le Teil earthquake (PGA 0.20 g) all necessitated extensive equipment inspections and prolonged outages despite minimal structural damage [1–4]. These cases highlight those not only actual failures, but also precautionary inspections lead to economic losses due to required plant shutdowns, which creates an urgent demand for methodologies that can predict equipment-level seismic responses rapidly to determine inspection priorities during or immediately after earthquake events.

Reliable seismic response prediction in NPPs faces a fundamental challenge involving two distinct types of uncertainty [5]. Aleatoric uncertainty reflects the inherent randomness of earthquake phenomena or material heterogeneity, whereas epistemic uncertainty arises from incomplete knowledge of material properties. Importantly, uncertainties in material properties may encompass both intrinsic variability (i.e., aleatory) and incomplete information (i.e., epistemic), depending on the context [6]. Uncertainties in GM have been studied extensively [7], but uncertainties in material properties have not attracted as much attention in the context of NPP research despite their critical importance. Recent studies have demonstrated that neglecting uncertainty about material

* Corresponding author.
** Corresponding author at: Division of Physical Metrology, Korea Research Institute of Standards and Science, 267 Gajeong-ro, Yuseong-gu, Daejeon 34113, Republic of Korea.
E-mail addresses: ylee@unist.ac.kr (Y.-J. Lee), jblee@kriss.re.kr, jblee@ust.ac.kr (J. Lee).

https://doi.org/10.1016/j.ress.2026.112582
Received 10 November 2025; Received in revised form 11 February 2026; Accepted 9 March 2026
Available online 10 March 2026
0951-8320/© 2026 The Authors. Published by Elsevier Ltd. This is an open access article under the CC BY-NC-ND license (http://creativecommons.org/licenses/by-nc-nd/4.0/).

properties can yield non-conservative fragility estimates [8]. Consistently, methodological frameworks for NPPs emphasize that such variability must be explicitly propagated to avoid overestimating the reliability of equipment [9].

Existing approaches for uncertainty quantification (UQ) involve considerable computational costs, which limits their applicability in real-time NPP safety assessment. Traditional Monte Carlo (MC)-based finite element (FE) simulations provide robust distributions but are computationally prohibitive for rapid decision-making. Alternative approaches including stochastic FE methods [10] and polynomial chaos expansions [11] offer improved efficiency but still cannot meet stringent time requirements. Recent machine learning (ML) and deep learning (DL) surrogate models have demonstrated substantial computational advantages in structural engineering such as predicting the shear capacity of structural components [12] and seismic performance [13,14].

In many recent DL studies, the target outputs are simplified scalar measures or specific response indices [15,16], rather than full time-history responses. More recently, efforts have expanded toward predicting richer response representations, including floor response spectra [17] and full response histories [18,19], as well as hybrid or physics-informed architectures for time-history prediction [20,21]. However, these real-time prediction models, including those leveraging transfer learning [22], often remain deterministic and do not explicitly quantify uncertainty. Moreover, they commonly assume fixed material properties and vary only the seismic input.

To bridge this gap by explicitly addressing the limitations of deterministic approaches and incorporating material uncertainty, we introduce an attention-enhanced multimodal deep learning (Att-MMDL) framework for predicting seismic floor responses in NPPs. The attention mechanism [23] demonstrates strong efficiency in processing long sequences and an excellent capability for fusing heterogeneous information and therefore has been actively applied in various studies. For instance, it has been utilized in remaining useful life (RUL) prediction [24–26] and for capturing interactions among heterogeneous features to predict damage parameters [27]. However, the use of the attention mechanism for fusing seismic and structural parameters to predict the full time-history of structural responses remains limited. In this study, two different types of input data are treated as distinct modalities, including (1) GM, represented as temporal sequences and encoded using a one-dimensional convolutional neural network (1D-CNN), and (2) structural parameters including density, Young's modulus, Poisson's ratio of concrete, and modal damping ratio, which are scalar data encoded using an artificial neural network (ANN) model. The two encoded features from the distinct modalities are then combined and passed to a 1D-CNN decoder, which reconstructs the acceleration responses at multiple equipment locations. This framework enables real-time probabilistic prediction of structural responses while simultaneously accounting for both seismic variability and uncertainties in structural parameters.

Multimodal learning refers to approaches that integrate different types of data such as images, text, video, or audio to perform specific tasks [28]. In this study, we considered GM and structural parameters as two separate modalities. Unlike conventional multimodal approaches that simply concatenate features from different modalities, the proposed framework incorporates a cross-modal attention mechanism [29] to capture the interdependence between the two separate modalities (i.e., sequence and scalar data). As a result, structural parameters adaptively influence the temporal patterns of GM while seismic features help determine the relative importance of different structural parameters. This design further enables the independent treatment of uncertainty in each modality, allowing the framework to propagate seismic variability and uncertainties in structural parameters separately through the prediction model.

2. Methodology

2.1. Overview of the proposed framework

The proposed framework comprises three sequential steps, as illustrated in Fig. 1, including (1) data generation through MC FE simulations, (2) training the Att-MMDL model, and (3) testing the model using independent datasets with GM and structural parameters that were not used during training.

The data generation process was performed using MC ABAQUS, which integrates MC simulation (MCS) with the FE software ABAQUS for systematic UQ. As shown in Fig. 2, the workflow comprised three primary components, including random sample generation, automatic modification of ABAQUS input files, and execution of simulations with response collection. We began by generating sample sets for random variables (RVs) based on their statistical distributions using MATLAB, which supports various probability distributions including normal, lognormal, exponential, and Gumbel. Each generated sample set automatically modified the original ABAQUS input file (i.e., *inp* file) by locating and replacing the corresponding RVs. ABAQUS simulations were then executed through DOS commands controlled by MATLAB, and a Python-based interface extracted structural responses (e.g., acceleration) from the output files (i.e., *odb* files). This automated framework efficiently produced comprehensive structural response datasets for diverse input scenarios for the subsequent uncertainty analysis.

The Att-MMDL model was trained using the generated dataset to simultaneously account for uncertainties arising from GM variability and structural parameters variability. The architecture consists of two encoder branches, including a 1D-CNN encoder for time-series GM data and an ANN encoder for scalar structural parameters. The key innovation is the incorporation of a cross-modal attention mechanism that enables adaptive interaction between seismic features as queries and structural parameters as keys and values. The fused representations are subsequently decoded using a 1D-CNN decoder to generate seismic response predictions at multiple equipment locations.

To ensure robust performance with unseen combinations of GM and structural parameters, the performance of the trained model was evaluated using an independent testing dataset that was not used in the training process. A set of 160 artificially generated GM sequences from a total of 206 were combined with 10 different combinations of structural parameters for training. In the first test scenario, 46 GMs paired with 10 combinations of structural parameters were used. To further assess the model's generalization capability with uncertainty of structural parameters, an additional second test scenario was evaluated with 100 combinations of structural parameters paired with 16 GMs from among the 46 used in the first test scenario.

Accordingly, 1600 data samples were utilized for the training phase. For the testing phase, 460 and 1600 data samples were employed step by step for the first and second scenarios, respectively. While data-driven approaches often require large datasets for training the model, the required sample size varies significantly depending on the type of problem, ranging from as few as 9 to as many as 1500 GMs even in the same task of seismic response prediction [22]. Thus, in this study, the number of data samples was determined based on the authors' empirical judgment and preliminary evaluations. This approach is designed to provide a comprehensive evaluation of the model's performance across varying structural parameters.

2.2. Target structure and its FE model

We applied the proposed Att-MMDL model to the auxiliary building of an NPP. A structural analysis model was developed using the ABAQUS FE software based on the reference model provided by the Korea Atomic Energy Research Institute (KAERI). The six-story auxiliary building was discretized into 17,233 shell elements, which primarily consisted of S4R

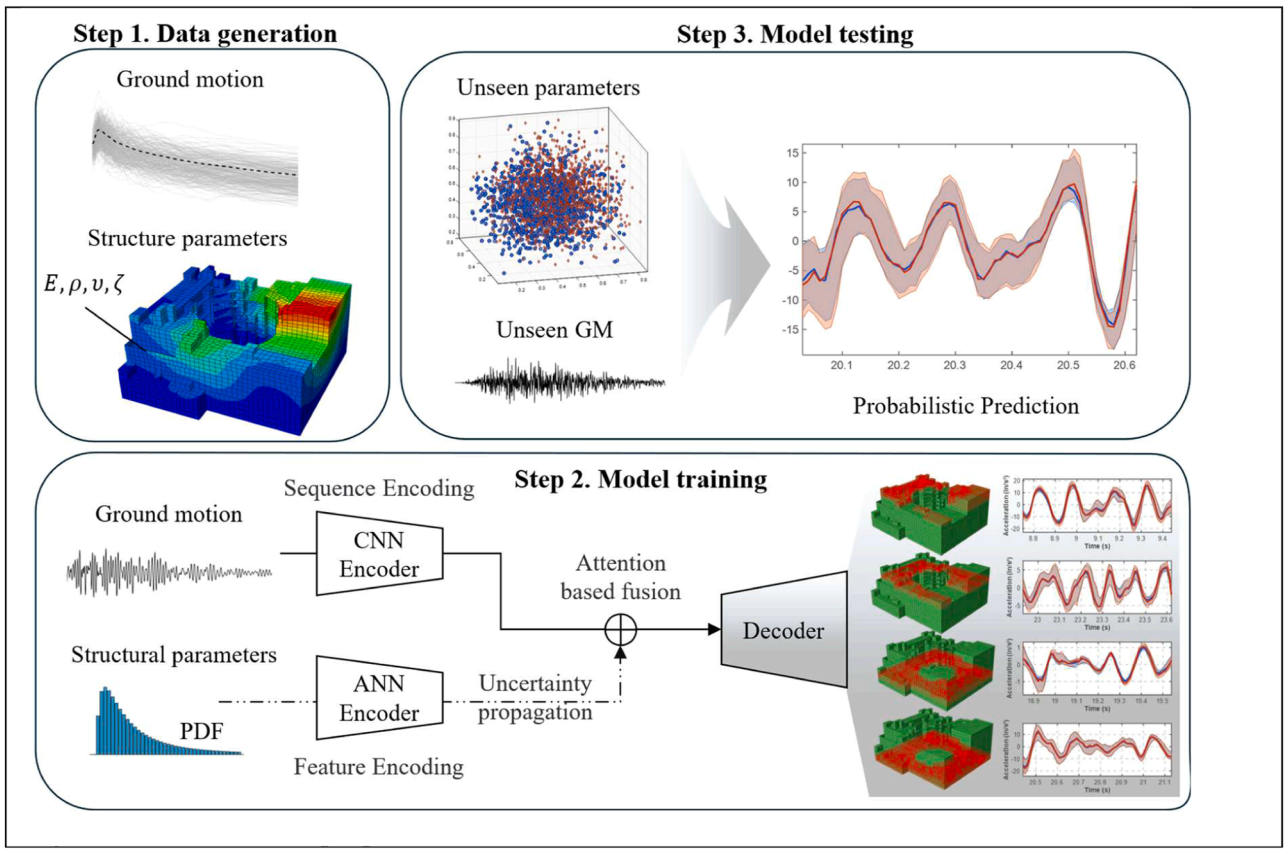

Fig. 1. Overview of the proposed framework.

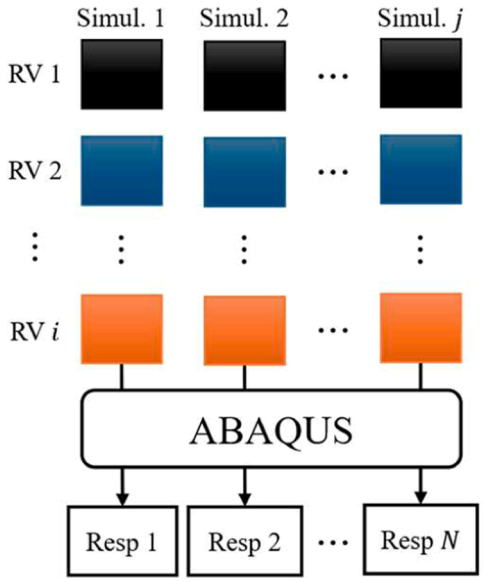

Fig. 2. Workflow of the MC ABAQUS framework.

elements (i.e., four-node shell elements) with a smaller portion of S3R elements (i.e., three-node shell elements). The model considers three types of material, including concrete, steel for reinforcing bars (rebars), and steel for non-rebar components, the properties of which are presented in Table 1. The structural analysis assumed linear elastic behavior, which is consistent with APR 1400 design criteria requiring elastic performance under Safe Shutdown Earthquake (SSE) events with a PGA of 0.3 g. The boundary conditions included full constraint at the

Table 1
Material properties of NPPs.

	Concrete	Steel	
		Rebar	others
Elastic modulus (psi)	4031,000	29,000,000	29,008,000
Density $(lbfs^2/in^4)$	0.000225	0.0007346	0.0007346
Poisson ratio	0.17	0.30	0.30

structural base, with seismic excitation applied in the horizontal plane (i.e., x-y direction) using time-acceleration input.

The auxiliary building consisted of seven structurally distinct parts, each characterized by unique geometric configurations, floor heights, and functional layouts. These interconnected sections form a complete

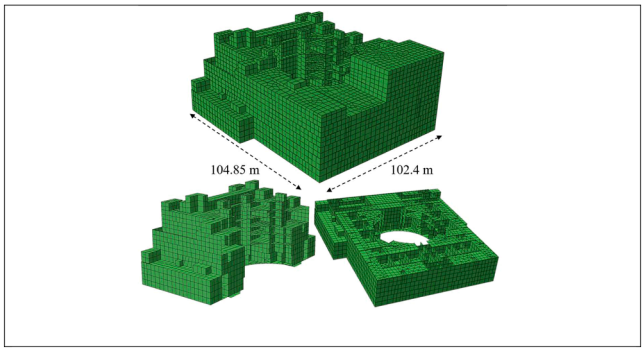

Fig. 3. Three–dimensional FEM of the auxiliary building: global configuration and internal sectional views.

structural system, as illustrated in Fig. 3. Fig. 4 presents a visualization of the FE model at different floor levels to show selected structural parts (i.e., Parts 1–7) that demonstrate the spatial variations for different floor levels. This structural complexity results in varying seismic responses even at identical floor levels. Although multi-location response is critical for understanding the effects on a wide variety of mechanical and electrical systems distributed throughout the structure, it can be very challenging to predict because of this variation.

The assumption of linear behavior was confirmed by conducting nonlinear pushover analyses in a single horizontal direction. These analyses revealed that the structure exhibited primarily linear characteristics until it reached a base shear coefficient of approximately 2 g, which substantially surpassed both the design PGA of 0.3 g and the spectral acceleration corresponding to the structure's fundamental period [30]. This establishes that the structural system remained within the elastic response range even when subjected to seismic forces considerably higher than those specified in the design criteria, which supports our adoption of a methodology based on linear dynamic analysis for this investigation.

The results of our investigation showed that although the structure operated within elastic limits, seismic loading could nonetheless lead to functional interruptions of essential equipment such as control systems, electrical distribution panels, power transformers, and backup generators. This underscores the critical requirement for precise response calculations across all areas of the facility. The dynamic structural responses were calculated using the mode-superposition method (MSM) with 100 vibrational modes. This technique breaks down the complex structural dynamic response into separate modal contributions to provide reliable response predictions for linearly elastic structural systems in a computationally efficient manner.

2.3. Uncertainty in structural parameters

To incorporate uncertainties into the time-series prediction framework, we considered the variability in structural parameters (i.e., density, Young's modulus, Poisson's ratio of concrete, and modal damping ratio). These structural parameters were represented as log-normally distributed random variables, which are appropriate for physical properties owing to their inherent nonnegativity and the realistic skewed distributions commonly observed in material testing [8,31].

The focus on concrete-related properties among the structural parameters is justified by the structural composition of the auxiliary building, which consists primarily of reinforced concrete elements. Because the global dynamic response of the structure is predominantly governed by concrete [32], the variability in steel properties was not explicitly modeled in the proposed framework. This simplification improves computational efficiency while still capturing the dominant sources of uncertainty [33,34].

To verify that the influence of steel property variability is negligible, we additionally evaluated the structural response under steel material uncertainties. Specifically, Young's modulus and Poisson's ratio of steel were modeled as random variables. Following the recommendations of JCSS [35], a log-normal distribution with a coefficient of variation of 0.03 was adopted, as summarized in Table 2. A total of 100 FE simulations were conducted using sampled combinations of steel material parameters under a single GM from the test dataset. As illustrated in Fig. 5, the resulting acceleration responses exhibit negligible variance, with the standard deviation remaining below 0.3 % of the maximum response amplitude even at the node showing the highest variability. These results confirm that the influence of steel property uncertainty on acceleration responses is negligible, thereby justifying the use of deterministic steel material properties in this study.

The statistical characteristics of the material properties of concrete and the modal damping ratio are summarized in Table 3, including the mean values and coefficients of variation. These values are derived from comprehensive experimental evidence and prior literature on structural parameter variability [36,37]. Following the framework proposed by Wang et al. [32], the Young's modulus, Poisson's ratio, and density of concrete, along with the modal damping ratio, were selected as material uncertainty parameters. The coefficients of variation for these parameters were set to 0.2, 0.1, 0.05, and 0.4, respectively, and each parameter was assumed to follow a log-normal distribution. Incorporating these uncertainties enables the proposed framework to account for both the

Table 2
Statistical characterization of structural parameters of steel for probabilistic analysis.

Structural parameters	Distribution	Mean	Coefficient of variation
Young's modulus	Log-normal	29,000,000 psi (rebar) 29,008,000 psi (others)	0.03
Poisson ratio	Log-normal	0.30	0.03

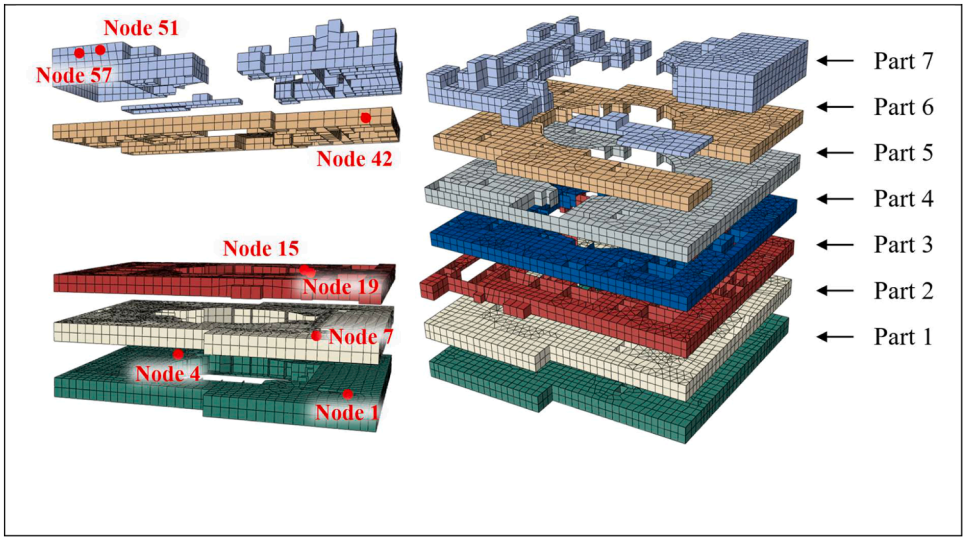

Fig. 4. FEM of the auxiliary building visualized at different floor levels. Left: nodes selected in Sections 2–4 to present the research results are marked; all nodes referenced throughout this paper are shown. Right: parts 1–7 represent the complete auxiliary building.

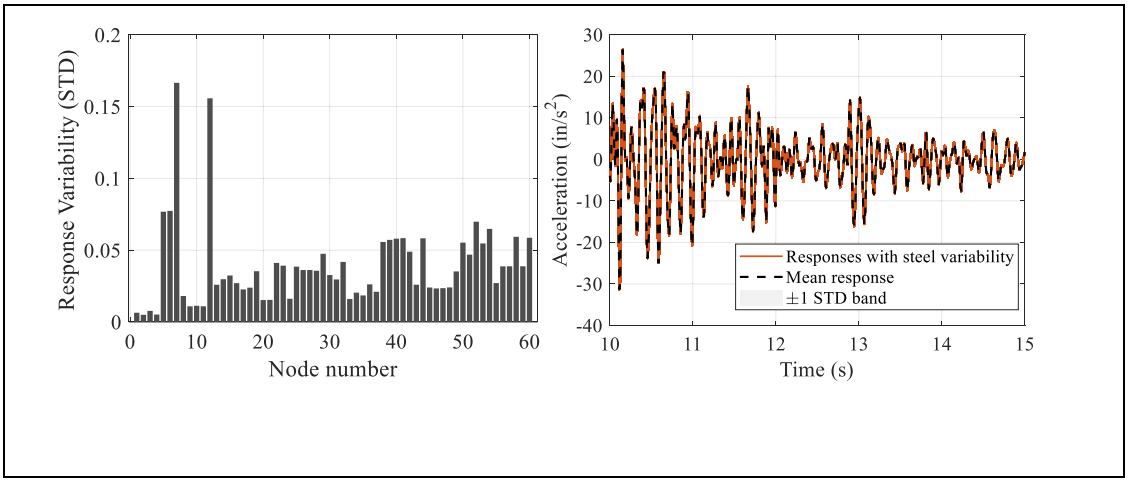

Fig. 5. Structural response uncertainty due to steel variations. Left: standard deviation (STD) of responses across nodes. Right: acceleration time-histories for 100 combinations of steel parameters at node 7 that shows maximum variability.

Table 3
Statistical characterization of structural parameters of concrete for probabilistic analysis.

Structural parameters	Distribution	Mean	Coefficient of variation
Young's modulus	Log-normal	4031,000 psi	0.20
Poisson ratio	Log-normal	0.17	0.10
Density	Log-normal	0.000225 lbf s^2/in^4	0.05
Modal damping ratio	Log-normal	0.07	0.40

inherent randomness of ground motion and structural variability, thereby providing a more comprehensive probabilistic reliability assessment of the predicted responses [38,39].

Conventional FE analysis (FEA)-based probabilistic analysis may require substantial computational cost to obtain stable estimates of probabilistic analysis results. In contrast, we adopted a data-driven strategy based on surrogate modeling in which a neural network is trained to generalize across the uncertainty space to avoid the need to compute the output statistics directly through FEA. For this purpose, we utilized a total of 206 GM sequences, of which 160 were allocated for training and the remaining 46 were reserved for evaluation. The training dataset consisted of 1600 samples (i.e., 160 GM sequences paired with 10 combinations of structural parameters). In addition, two complementary testing scenarios were constructed to assess generalization under different uncertainty conditions: (1) 460 samples (i.e., 46 GMs paired with 10 combinations of structural parameters) and (2) 1600 samples (i.e., 16 GMs paired with 100 combinations of structural parameters). These scenarios were designed to evaluate the surrogate model's ability to generalize to unseen ground motions and to broader variations in structural parameters, respectively. To incorporate uncertainty in structural parameters systematically, we generated multiple combinations of statistically varied structural parameters that were applied consistently during both training and testing phases.

2.4. Proposed network architecture

The architecture of the proposed Att-MMDL framework is illustrated in detail in Fig. 6. For a comparative analysis, we used multimodal baseline models as the reference framework. Here, *multimodal* refers to the use of two heterogeneous types of input data, including (1) data on GM, which is provided as time-dependent sequences, and (2) structural parameters, which are given as scalar values. By combining these distinct input modalities, the proposed structure integrates cross-modal attention mechanisms with convolutional autoencoder architectures [40]. This design enables the framework to combine information from two distinct modalities effectively to predict seismic responses at multiple structural locations more accurately than the baseline model, which combines information using simple concatenation.

The GM data are processed using a residual 1D CNN (Res-1D CNN) based encoder that extracts temporal patterns and frequency features from seismic signals. The encoder consists of multiple residual blocks with progressively decreasing kernel sizes and increasing filter numbers, where each residual block processes the seismic features h_s at layer l [19]. The residual connection is implemented as

$$h_s^l = Swish\left(h_s^{l-1} + BN\left(Conv1D\left(BN\left(Conv1D\left(h_s^{l-1}\right)\right)\right)\right)\right),$$

where h_s^l represents the seismic features in layer l, *Conv1D* is a 1D convolutional layer, *BN* denotes batch normalization, and *Swish* is the activation function. This ensures effective gradient flow and feature preservation throughout the encoder. This residual structure prevents the vanishing gradient problem and allows the network to learn seismic patterns effectively. The final seismic features are projected onto the attention dimension and combined with sinusoidal positional encoding to preserve the temporal information that directly passes through the input GM:

$$Q = W_q \cdot Swish\left(BN\left(h_s^{final}\right)\right) + PE,$$

where Q represents the query matrix for the attention computation, W_q is the query projection matrix, h_s^{final} denotes the final seismic features from the encoder, and *PE* represents a sinusoidal positional encoding. The positional encoding ensures that the temporal sequence information of the GM data is preserved during the attention computation. The seismic features from the encoder and PE play the role of queries in multi-head attention module.

In parallel, the structural parameters, including density, Young's modulus, the Poisson's ratio of concrete, and the modal damping ratio are processed through an ANN-based encoder. The structural parameters x_p are passed through fully connected layers with batch normalization and Swish activation as given below.

$$h_p = Swish(BN(W_p \cdot x_p + b_p)),$$

where h_p represents the encoded information on structural parameters, x_p denotes the four structural parameters, and W_p and b_p are the weight matrix and bias vector of the fully connected layer, respectively. This

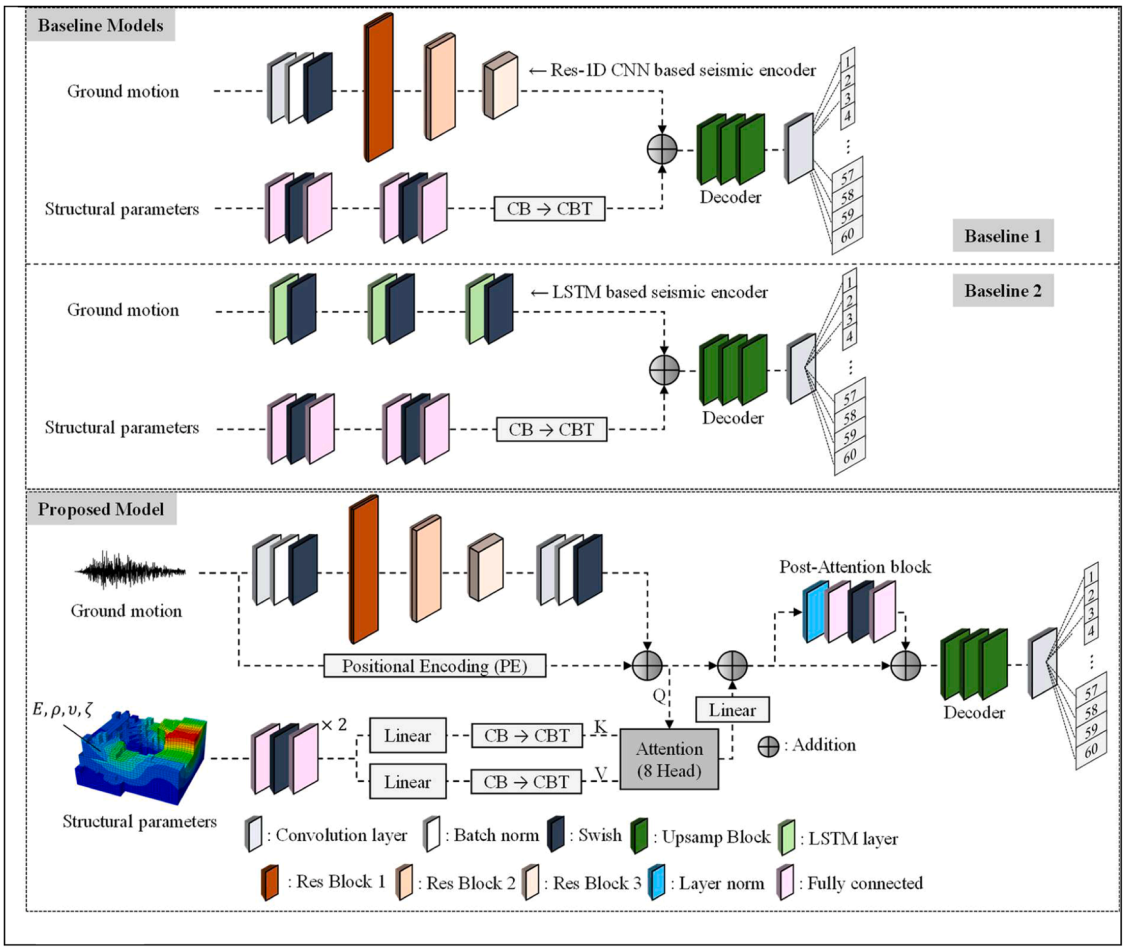

Fig. 6. Proposed network architecture.

encoding transforms the structural parameters into a latent space where they can effectively interact with seismic features from the Res-1D CNN based encoder. The encoded information (i.e., h_p) is then transformed into keys and values for the attention computation, in which the features are reshaped from the $[C \times B]$ to $[C \times B \times 1]$ format for temporal conditioning.

$$K = CB2CBT(W_k \cdot h_p),$$

$$V = CB2CBT(W_v \cdot h_p),$$

where K and V represent the key and value matrices for the attention computation, W_k and W_v are the projection matrices for keys and values, respectively; and *CB2CBT* stands for channel batch to channel batch time reshaping. This operation that aligns the features obtained from structural parameters with the temporal dimension of GM data to compute cross-modal attention.

The core innovation lies in the cross-modal attention mechanism, which allows data of the two modalities of GM and structural parameters to interact adaptively to selectively emphasize the most relevant structural parameters in response to varying GM characteristics.

$$head_i = softmax\left(\frac{Q_i K_i^T}{\sqrt{d_k}}\right) V_i,$$

where $head_i$ represents the i-th attention head, Q_i, K_i, V_i are the query, key, and value matrices for the i-th head, respectively, d_k is the dimension of the key vectors, and T denotes the matrix transpose. The GM data are formulated as queries, while the structural parameters serve as keys and values. The model quantifies the degree of relevance between specific GM patterns and individual structural parameters as the dot product of the query and the key. The *softmax* function creates attention weights that determine the extent to which each structural parameter should influence the response prediction for different seismic patterns. The final attention output combines all heads as

$$Attention(Q, K, V) = Concat(head_1, \ldots, head_h)W^O,$$

where h represents the number of attention heads, *Concat* denotes the concatenation operation, and W^O denotes the output projection matrix. This multi-head attention extends the basic attention mechanism by running multiple attention operations in parallel, allowing each head to independently capture similarities in the cross-modal relationships between GM and structural parameters. The outputs from all the heads are then concatenated and linearly transformed with the output projection matrix to obtain a unified representation that integrates diverse patterns. The attention output is processed through residual connections and a feedforward block to refine the fused features. The first residual connection combines the original query with the attention output.

$$Z_1 = Q + Swish(W_1 \cdot Attention(Q, K, V) + b_1,$$

where Z_1 represents the first intermediate representation after the residual connection. This step preserves the original GM features while incorporating the attention features conditioned by the structural parameters. This is followed by layer normalization and a feedforward network with another residual connection.

$$Z_2 = Z_1 + FFN(LayerNorm(Z_1)),$$

where Z_2 is the final fused representation, *LayerNorm* denotes layer normalization, and *FFN* represents the feedforward network (i.e., the post-attention block in Fig. 6). The feedforward network consists of two linear transformations with Swish activation and dropout.

$$FFN(x) = W_2 \cdot Dropout(Swish(W_1 \cdot x + b_1)) + b_2,$$

where W_1, b_1, W_2, b_2 are the weights and biases of the two linear layers and *Dropout* represents the dropout regularization operation.

Finally, the fused features are reconstructed into multi-location seismic responses through a decoder composed of upsampling and 1D convolutional layers. Each decoder layer progressively increases the temporal resolution through

$$y^l = Swish(BN(Conv1D(Upsample(y^{l-1}, r_l)))),$$

where y^l represents the output at decoder layer l, y^{l-1} is the input from the previous layer, r_l represents the upsampling ratio at layer l (with a value of 1 in this model), *Upsample* denotes the upsampling operation, and *Conv1D* represents a one-dimensional convolution. Each decoder layer reconstructs higher-resolution temporal features, and the model gradually builds up the detailed seismic response patterns. The final output layer produces responses at 60 structural locations.

$$y_{out} = Conv1D(y^{final}, 1, 60),$$

where y_{out} is the final predicted seismic responses, y^{final} represents the features passed through the final decoder layer, and the numbers 1 and 60 respectively indicate the kernel size and number of output channels (i.e., structural locations). This final layer maps the processed features to 60 spatial locations to provide comprehensive predictions of structural response across the entire structure. This hybrid architecture is designed to effectively capture the complex mapping between seismic inputs and spatially distributed structural responses while explicitly modeling uncertainties arising from GM and structural parameters through the attention-enhanced multimodal fusion mechanism.

2.5. Hyperparameters for the proposed and baseline models

Table 4 lists the hyperparameters for the proposed and baseline models. The baseline models share the same structural parameter encoder and decoder architecture but differ in how the GM input is processed and how seismic and structural features are fused. Specifically, baseline model 1 employs a Res-1D CNN-based seismic encoder, whereas baseline model 2 adopts an LSTM-based seismic encoder. The Res-1D CNN encoder used in baseline model 1 and the proposed model was inspired by Lee [41], which investigated seismic response prediction for the same auxiliary building of NPPs and showed that progressively decreasing the kernel size while increasing the number of filters enables more effective feature extraction from GM sequences than alternative CNN configurations. Accordingly, both baseline model 1 and the proposed model adopt a Res-1D CNN encoder structure. To ensure a fair comparison, all models use the same input configuration consisting of one-dimensional GM sequences and four structural parameters, and they share an identical decoder to maintain consistent output reconstruction capacity. In addition, the number of filters in the seismic encoder and decoder is kept consistent across models to isolate the impact of architectural design. For feature fusion, both baseline models apply element-wise addition, since feature concatenation showed inferior performance in preliminary experiments.

3. Model training

To train and evaluate the proposed model, we constructed a dataset using the MC ABAQUS framework as described in Section 2.1. The dataset consisted of 206 artificially generated sequences of data on GM which has sampling rate of 100 Hz and a total duration of 30 s to simulate a wide range of GM scenarios with varying frequencies and amplitudes. The artificial earthquake (AEQ) data were generated by using the stochastic GM model developed by Rezaeian and Der Kiureghian [42]. To reflect the nonstationary nature of actual seismic records, this model represents ground acceleration as a modulated gaussian process with time-varying amplitude and frequency. Crucial parameters defining the amplitude envelope and frequency evolution, including the Arias intensity (I_a), significant duration (D_{5-95}), and central frequency (ω_{mid}) were derived through seismological predictive equations. For a case study of the Ulsan city, where APR1400 NPPs are situated, specific seismic variables were adopted: a strike-slip fault ($F = 0$), a moment magnitude of $M = 6.0$, a rupture distance of $R_{rup} = 40\ km$, and $V_{s30} = 715\ m/s$. These site-specific inputs were integrated into regression models to establish the statistical framework for synthetic GM generation.

The spectral accelerations of the GMs used for training and testing are illustrated in Fig. 7. Although the spectra used for testing fell within the overall range of the spectra allocated for training, some exhibited distinct spectral shapes.

As mentioned in Section 2.3, 206 GMs were used to construct the dataset. Among them, 160 GMs were used for training, while the remaining 46 GMs were used for testing. During training, each of the 160 GMs was combined with 10 randomly sampled structural parameter sets, resulting in 1600 training samples. Each data sample consists of a GM input with a dimension of $3,000 \times 1 \times 1$ and a corresponding structural parameter vector of size 4×1. The output represents time-history responses at 60 spatial locations, resulting in an output

Table 4
Hyperparameter settings for comparative study.

Category	Hyperparameter	Baseline 1	Baseline 2	Proposed Model
Input channels	Ground Motion	1 (Sequence)	1	1
	Structural Parameters	4 (Features)	4	4
Seismic Encoder	Layer Type	Res-1D CNN blocks	LSTM	Res-1D CNN blocks
	Filters / Hidden Units	32, 64, 128	32, 64, 128	32, 64, 128
	Kernel Size	k, k/2, k/8 ($k = 64$)	-	k, k/2, k/8
	Positional Encoding	-	-	Sinusoidal
Structural Encoder	FC Layers (Units)	32, 128	64, 128	64, 128
Fusion / Attention	Mechanism	Element-wise Addition	Element-wise Addition	Multi-head Attention
	Attention Dim / Heads	-	-	128 / 8 Heads
	FFN Hidden Dim	-	-	512, 128
	Dropout Rate	-	-	-
Decoder	Layer Type	1D Conv + Upsample	1D Conv + Upsample	1D Conv + Upsample
	Filters	128, 64, 32	128, 64, 32	128, 64, 32
	Kernel Size	k/8, k/2, k	k/10, k/2, k	k/8, k/2, k
Output	1×1 Conv	60	60	60
Num of parameters	-	1.2 M	663.9 K	1.2 M

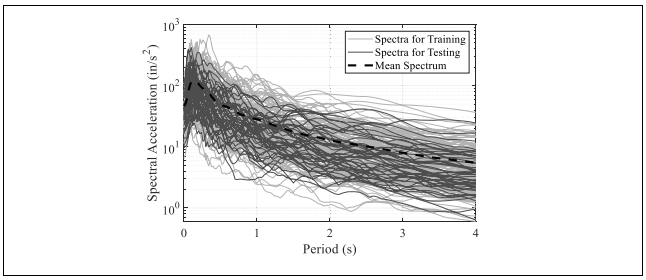

Fig. 7. Comparison of spectra for training and testing with the mean spectrum.

dimension of $3,000 \times 60 \times 1$. The test dataset was evaluated under two scenarios: (1) combining all 46 test GMs with 10 structural parameter sets to generate 460 samples, and (2) combining a subset of 16 test GMs with 100 randomly generated structural parameter sets to generate 1600 samples.

Hyperparameters, including the initial learning rate, mini-batch size, and L2 regularization coefficient, were selected through grid search over $\{0.001,\ 0.005,\ 0.01\}$, $\{64,\ 128,\ 256\}$, and $\{10^{-4},\ 10^{-3},\ 10^{-2}\}$, respectively. The final model was trained using the Adam optimizer with a learning rate of 0.001 and a mini-batch size of 256 for 1200 epochs, with shuffling applied at each epoch. Gradient clipping with an L2-norm threshold of 1.0 was used for stable convergence, the learning rate was decayed by a factor of 0.9 every 350 epochs, and L2 regularization with $\lambda = 1 \times 10^{-3}$was employed to mitigate overfitting.

4. Results and discussion

Two distinct testing scenarios were designed to evaluate the proposed model under combined uncertainties in GM inputs and structural parameters, while emphasizing different dominant sources of variability. The first scenario primarily assesses the model's generalization capability under seismic input uncertainty by examining whether it can accurately predict structural responses to previously unseen GMs, with structural parameter uncertainty treated as a secondary factor. The second scenario, in contrast, focuses on structural parameter uncertainty by evaluating how sensitively and consistently the model responds to variations in structural parameters under a limited set of seismic inputs.

4.1. Model testing scenario 1

To evaluate the robustness of the proposed model under seismic input uncertainty, 460 data samples were constructed by combining 46 unseen GMs with 10 unseen combinations of structural parameters. The performance of the model was evaluated using two error metrics, including maximum mean absolute percentage error (mMAPE) [43] and the coefficient of determination (R^2). The mathematical formulations for these error metrics are given as follows.

$$mMAPE = \left\{ \frac{100}{n} \sum_{t=1}^{n} \frac{|A_t - F_t|}{|A|_{max}}, \right.$$

$$R^2 = 1 - \frac{\sum_{t=1}^{n} (A_t - F_t)^2}{\sum_{t=1}^{n} (A_t - \overline{A})^2},$$

where A_t and F_t denote the actual and predicted responses at time step t, respectively, $\overline{A}$ represents the mean of the actual responses, n is the total number of time steps, and $|A|_{max}$ indicates the maximum absolute value among the actual responses. The mMAPE normalizes the error with the magnitude of the peak response to provide a more interpretable percentage-based error. The R^2 value quantifies the proportion of variance in the actual data, which is explained by the model predictions. Together, they provide a comprehensive framework for evaluating the performance of the model performance under conditions of varying uncertainty.

Fig. 8 compares the predicted and FE-simulated acceleration responses to evaluate the performance of the model with uncertainty as to seismic input. Each subplot visualizes a randomly selected time segment corresponding to a varied GM and 10 combinations of distinct structural parameters. The predicted responses demonstrate strong agreement with the FE simulations in terms of both amplitude and phase characteristics, and the trained model successfully captured the phase shift and amplification of the responses.

The obtained values of R^2 are compared in Fig. 9 and Fig. 10. These results demonstrate that the proposed model performed better than the baseline. Although the baseline model shares a similar overall architecture (i.e., Fig. 6), the key distinction lies in the fusion of different modalities. The proposed model incorporates cross-modal attention mechanisms to capture more comprehensive relationships between seismic features and structural parameters, whereas the baseline model uses conventional concatenation-based methods.

Fig. 9 and 9 together provide a comprehensive evaluation of the baseline and proposed models. The bivariate density contour plots in Fig. 9 compare predicted and reference responses, with baseline model 1 shown on the left, baseline model 2 in the middle, and the proposed model on the right. The plots were constructed from log-scaled density estimates of the joint distribution of the predicted and reference responses. Contour lines delineate regions of higher density to show the agreement between predictions and references in terms of amplitude and phase characteristics. In both plots, the predictions were concentrated along the diagonal line (i.e., $y = x$), which indicates good agreement. The proposed model exhibited noticeably tighter clustering around the diagonal compared to the baseline, as reflected in higher coefficients of determination (i.e., $R^2 = 0.96$ for baseline 1, $R^2 = 0.94$ for baseline 2 and $R^2 = 0.98$ for the proposed model). This improvement indicates that the proposed model captured a substantially larger proportion of the variance in the structural response data and reduced systematic deviations relative to the baseline models.

Building on this aggregate validation, Fig. 10 shows the prediction errors across the 60 nodes. The left subplot shows the node-wise mMAPE for the baseline model, while the right subplot shows those for the proposed model. The mean node-wise time-averaged mMAPE across all 60 nodes was 2.24 % for baseline model 1, 3.13 % for baseline model 2, and 1.03 % for the proposed Att-MMDL model, corresponding to error reductions of 54.02 % and 67.09 % relative to baseline models 1 and 2, respectively. These consistent lower errors across all nodes demonstrate that the proposed model achieved significantly improved relative accuracy and generalized both the global behavior of NPPs and the local node-specific dynamic behaviors effectively. This spatial robustness is particularly valuable for applications such as structural health monitoring and seismic risk assessment.

Taken together, the findings shown in Fig. 9 and Fig. 10 highlight the superior performance of the proposed model compared to the baseline models in terms of both global agreement and local spatial accuracy. Combined with the time-history comparisons in Fig. 8, these results confirm that the proposed model provided accurate, generalizable, and computationally efficient predictions of seismic response under diverse GMs.

4.2. Model testing scenario 2

To evaluate the generalization capability of the model under varying uncertainty of structural parameters, we designed a test scenario in which the structural parameters varied extensively by combining 100 combinations of distinct sets of structural parameters with 16 GMs. Unlike the previous experiment, which emphasized uncertainty in seismic input, this setup reduced the number of GMs from 46 to 16 while substantially increasing the number of structural parameters per GM

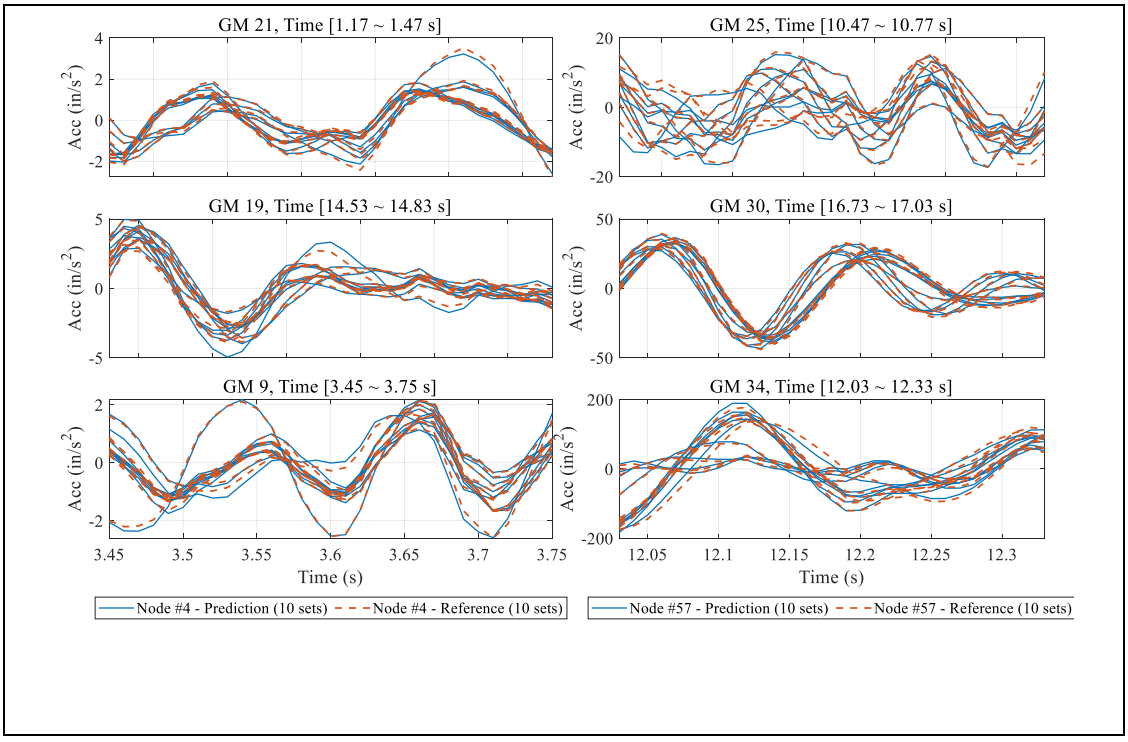

Fig. 8. Representative time-history comparisons between FE simulation data (i.e., reference) and model predictions for a selected GM. Each subplot corresponds to one of the 10 different combinations of structural parameters, while the seismic input remains constant.

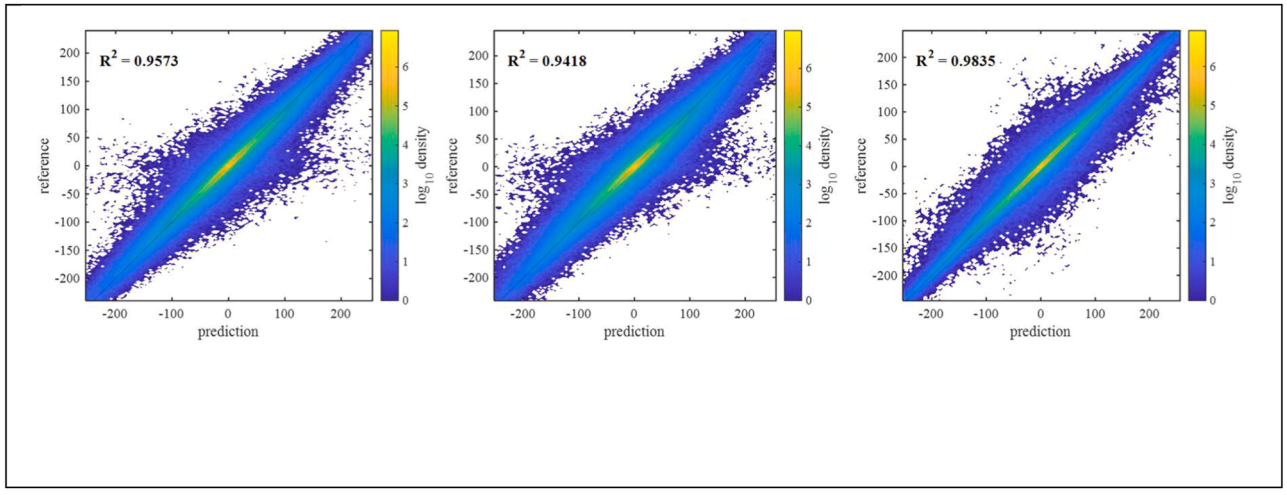

Fig. 9. Bivariate density of predicted vs. reference acceleration for all 60 nodes. Colors indicate log-scaled sample density, and the dashed line denotes the ideal prediction (i.e., $y = x$). Left: baseline model 1, R^2=0.96. Middle: baseline model 2, R^2=0.94. Right: proposed Att-MMDL model, R^2=0.98.

data sequence from 10 to 100. Here, we focused more on uncertainty in structural parameters.

Fig. 11 presents time-history comparisons of the predicted and FE-simulated acceleration responses at Nodes #15 and #42 evaluated across 100 sets of structural parameters and three representative sequences of GM. For each case, a randomly selected time segment is shown, where solid lines indicate predictions and dashed lines represent the FE references. The results demonstrate that the predictions closely followed the references, successfully reproducing both amplitude and phase characteristics across a wide range of structural parameter variations. This agreement highlights the capability of the model to generalize effectively, which supports its potential as a computationally efficient surrogate for intensive FE simulations with varying structural parameters of concrete and damping uncertainties.

Building on these comparisons, Fig. 12 further evaluates the model's ability to capture the statistical distribution of responses under uncertainty. Each subplot depicts the interquartile range (IQR) and median of the predicted and reference acceleration responses across 100 combinations of structural parameters with variations subjected to the same GM. The shaded regions correspond to the IQR, while solid lines represent the median responses. The obtained predictions (i.e., blue lines) and references (i.e., orange lines) exhibit strong alignment, with the predicted distributions closely matching the distribution of the FE-based responses. This consistency demonstrates that the model not only preserves accuracy at the individual response level but also captures the characteristics of structural behavior with varying uncertainty

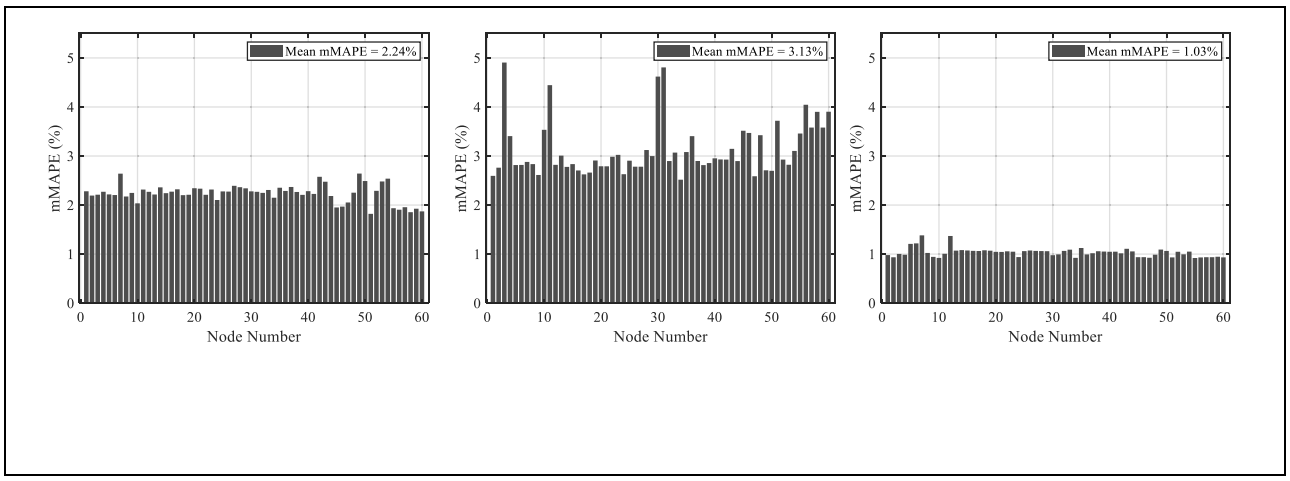

Fig. 10. Node-wise prediction error (i.e., mMAPE) for all 60 nodes. Gray bars show time-averaged mMAPE per node. Left: baseline model 1, mean mMAPE = 2.24 %. Middle: baseline model 2, mean mMAPE = 3.13 %. Right: proposed Att-MMDL model, mean mMAPE = 1.03 %.

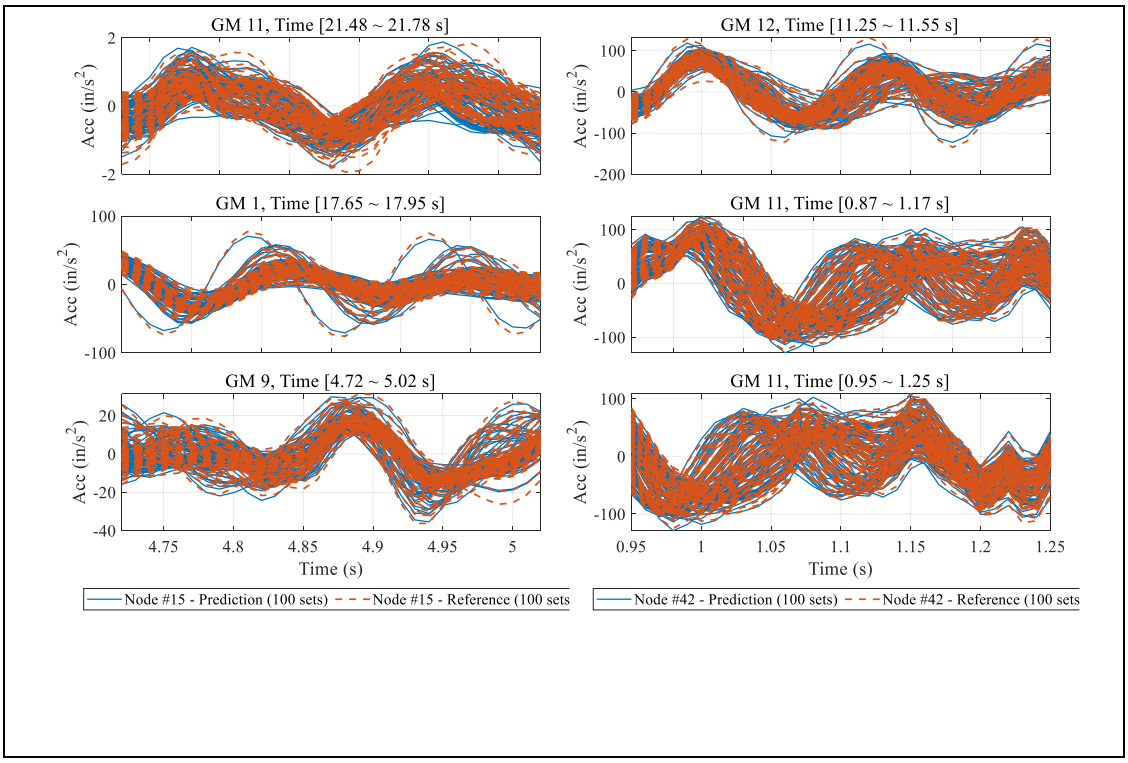

Fig. 11. Time-history comparison of predicted and reference acceleration responses at Node #15 and Node #42, evaluated across 100 structural parameters sets under three representative GMs. For each case, a randomly selected time segment is shown. Solid lines denote the predicted responses, while dashed lines indicate the FE reference simulations.

about structural parameters.

Following this statistical evaluation, Fig. 13 presents two-dimensional density contour plots as described above in Section 4.1 that visualize the relationship between the predicted and reference responses to provide an intuitive perspective on the model's overall performance. Two subsets are shown to evaluate the model's performance across different value ranges; the left and middle panels show the baseline models 1 and 2, respectively, while the right panel shows the proposed Att-MMDL model. Baseline models 1 and 2 exhibited strong correlations with R^2=0.96 and R^2=0.94, respectively; however, the point clouds showed noticeable dispersion around the diagonal line, indicating prediction deviations across the response range. In contrast, the proposed model achieved a higher agreement with R^2=0.99, with data points clustering more tightly along the diagonal, confirming improved predictive accuracy and reduced bias.

Building on this global evaluation, Fig. 14 provides a node-wise error comparison among the baseline models and the proposed model using the mean mMAPE values. Each bar represents the time-averaged error at an individual node across all testing datasets. Baseline model 1 and baseline model 2 yielded mean mMAPE values of 2.02 % and 2.58 %, respectively, with several nodes exhibiting relatively higher errors. In contrast, the proposed Att-MMDL model achieved a substantially lower mean mMAPE of 0.95 %, showing consistently reduced errors across all nodes and mitigating the high-error outliers observed in the baseline

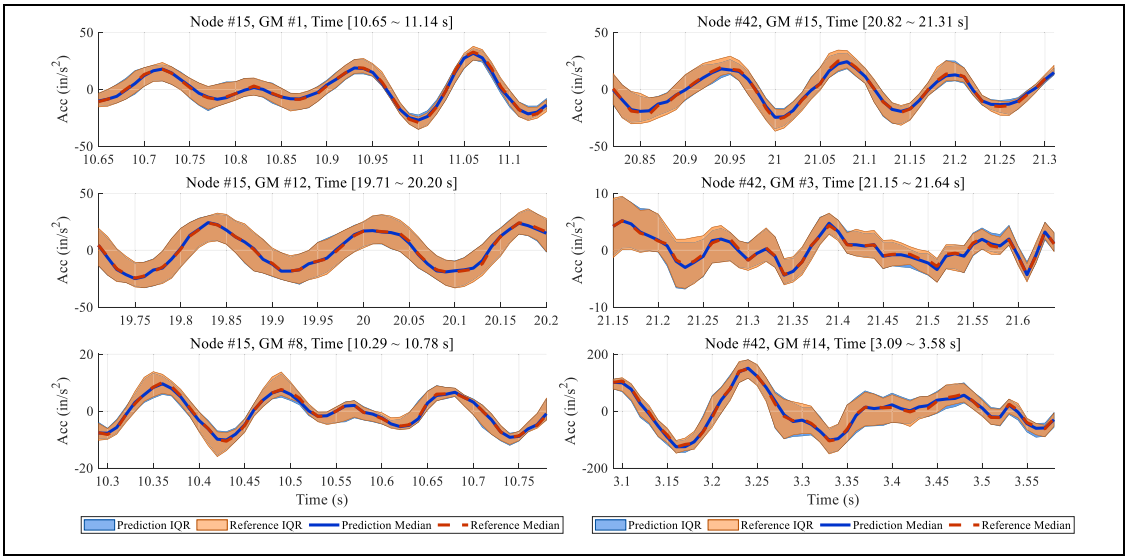

Fig. 12. Statistical comparison of predicted and reference acceleration responses under structural parameters uncertainty. Each subplot shows the median and interquartile range (IQR, 25th–75th percentile) of responses across 100 combinations of structural parameters sets subjected to the same GM. For each case, a short time segment is randomly selected to illustrate temporal variability. Shaded regions indicate the IQR, and solid lines represent the median responses, with blue corresponding to predictions and orange to references.

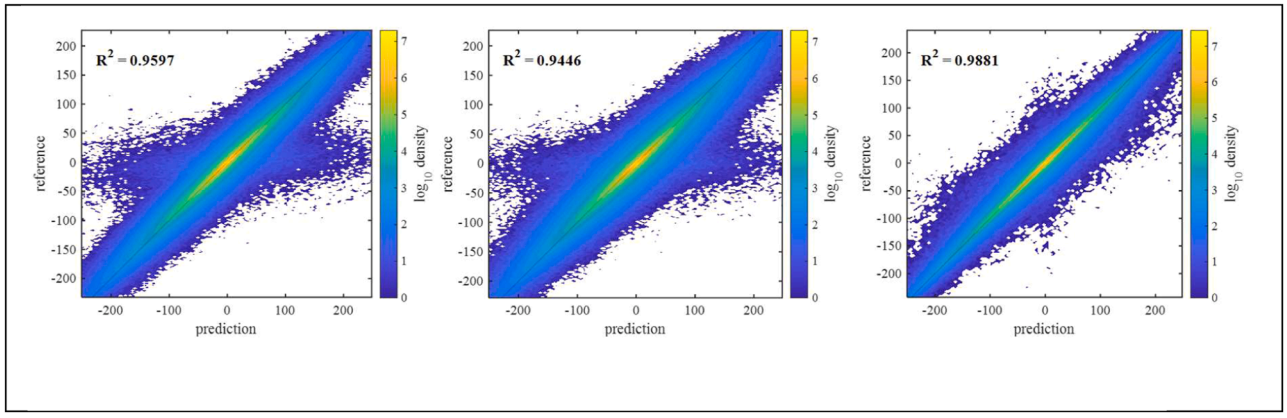

Fig. 13. Bivariate density of predicted vs. reference acceleration for all 60 nodes. Left: baseline model 1, R^2=0.96. Middle: baseline model 2, R^2 = 0.94. Right: proposed Att-MMDL model, R^2= 0.99.

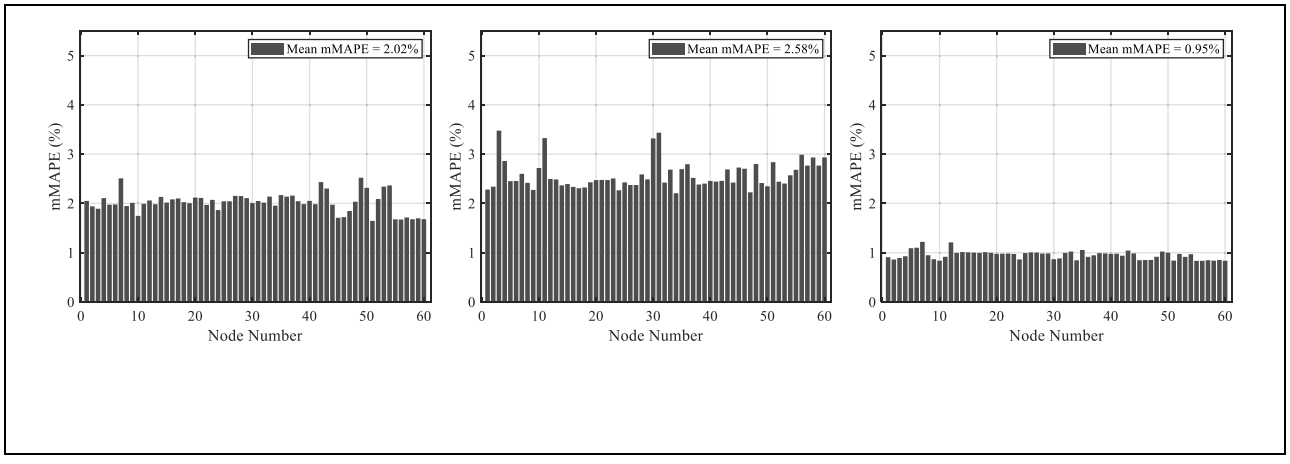

Fig. 14. Node-wise prediction error (mMAPE) for all 60 nodes. Gray bars show time-averaged mMAPE per node. Left: baseline model 1, mean mMAPE = 2.02 %. Middle: baseline model 2, mean mMAPE = 2.58 %. Right: proposed Att-MMDL model, mean mMAPE = 0.95 %.

cases. Overall, these results indicate that the proposed model improves predictive accuracy while maintaining spatially consistent performance across nodes under diverse and uncertain conditions.

Taken together, the results from the two testing scenarios demonstrate that the proposed framework can generate large ensembles of probabilistic structural response time histories without requiring repeated high-cost simulations. The model maintained accurate predictions under variability in seismic inputs and uncertainty in structural parameters, supporting its use as a practical surrogate for response prediction with substantial computational savings. Moreover, its real-time inference capability enables seamless integration into downstream applications such as probabilistic safety assessment (PSA) and fragility analysis. For NPP auxiliary buildings, this framework facilitates risk-informed fragility evaluation of equipment distributed across different elevations and locations, including emergency diesel generators, electrical panels, and piping systems, where reliable seismic response prediction is essential for nuclear safety assessments.

4.3. Robust prediction across ground motions with diverse effective durations

Importantly, the proposed model was trained and evaluated using GMs with a wide range of effective durations, as demonstrated in Fig. 15. As discussed in Section 4.2, the model consistently exhibited strong predictive performance across the test dataset, despite substantial variability in effective duration.

Although the input GMs and corresponding structural responses are represented using a total duration of 30 s in this study, the results indicate that the model performance is not confined to a single duration characteristic. Instead, the framework demonstrates robust predictive capability across ground motions with diverse effective durations, supporting its applicability to seismic inputs with varying duration characteristics.

4.4. Interpretability and sensitivity analysis via attention mechanism visualization

To investigate the internal process of the proposed Att-MMDL model, the attention mechanism was analyzed as illustrated in Fig. 16. This visualization provides a quantitative and interpretable basis for understanding how the model adaptively prioritizes seismic features and structural parameters during response prediction.

The top panel of Fig. 16 shows the ground motion input (i.e., test No. 2) and the query-path heatmap, which represents the magnitude of query features extracted from the GM through the attention mechanism. Notably, regions of high activation intensity (i.e., highlighted in light grey) are well aligned with the strong-motion duration of the earthquake. This indicates that the model selectively amplifies important temporal features of the seismic input, reflecting a *time-dependent sensitivity* to strong excitation phases that are important for accurate structural response prediction.

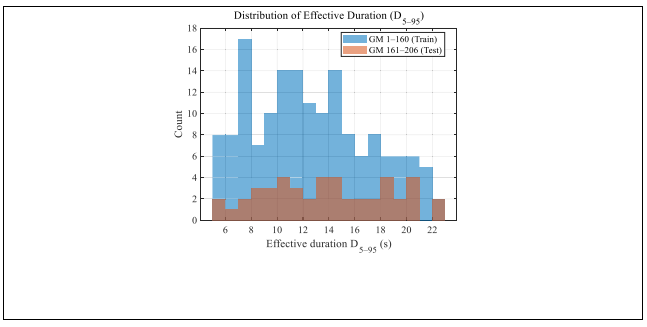

Fig. 15. Comparison of effective duration (D_{5-95}) between training and test GMs. Histograms show the distributions for GM 1–160 (training set) and GM 161–206 (test set) based on 30 s input GMs.

The bottom panel illustrates the adaptive parameter influence derived from the query–key interaction, which can be interpreted as a *time-dependent relative sensitivity* of the predicted response to individual structural parameters. Rather than exhibiting static importance, attention weights reveal a clear temporal evolution in parameter sensitivity over the path of the GM. In particular, the influence associated with Young's modulus, which governs structural stiffness, shows moderate fluctuations during the strong-motion phase and remains consistently non-negligible throughout the seismic event. Meanwhile, as the ground motion amplitude decays, the sensitivity gradually shifts toward damping-related properties, with the modal damping ratio becoming increasingly prominent in the later stage, suggesting a transition from excitation-driven response behavior to decay-dominated characteristics. Notably, the influence of density decreases gradually after 15 s and drops more sharply beyond approximately 20 s, suggesting reduced sensitivity to inertia-related effects as the input excitation weakens. In contrast, Poisson's ratio exhibits a relatively stable influence throughout the event with only minor variations, indicating its limited contribution to global seismic response characteristics. Overall, the observed temporal evolution of parameter influence suggests that the proposed Att-MMDL framework captures regime-dependent patterns in parameter relevance, rather than relying on static parameter weighting.

4.5. Risk quantification application

In this case study, the proposed model was applied to quantify seismic risk of critical equipment in NPPs through a real-time probabilistic assessment. In contrast to deterministic approaches that provide binary risk classifications for a specific threshold, the proposed model was introduced to generate probabilistic predictions using the uncertainty information of GM and structural parameters.

The key innovation lies in the real-time calculation of exceedance probabilities. The temporal exceedance probability is computed as follows.

$$P_{exc}(t) = \frac{1}{100}\sum_{i=1}^{100} \mathrm{I}(a_i(t) > a_{threshold}),$$

where $\mathrm{I}(\cdot)$ is the indicator function, which takes the value of 1 when the condition is satisfied and 0 otherwise, and $a_i(t)$ represents the acceleration response at t.

The left panels of Fig. 17 show the predictions provided by the deterministic and probabilistic approaches. The right panels of Fig. 17 compare the $P_{exc}(t)$ for the deterministic and probabilistic predictions for the same GM applied to different node locations, and the results show fundamental differences in their risk assessment capabilities. In the deterministic prediction, $P_{exc}(t)$ is evaluated from a single prediction at each time step and therefore takes only binary values of 0 or 1. Both acceleration responses from the deterministic prediction at Nodes 1 and 4 did not exceed the threshold, resulting in identical $A_{deter} = 0.00$ (i.e., the area under $P_{exc}(t)$ based on the deterministic prediction). Under deterministic assessment, both nodes would be classified as equally safe, which provides no basis for inspection prioritization. However, the probabilistic prediction based on the proposed Att-MMDL model revealed substantial differences in risk levels: Node 1 exhibited an A_{prop} value (i.e., the area under $P_{exc}(t)$ based on the probabilistic prediction) of 0.28, whereas Node 4 had an A_{prop} of 0.16. This difference represents a higher risk for Node 1, indicating that accounting for uncertainties in the structural parameters provided useful information for decision-making despite identical risk classifications under deterministic assessment.

The results shown in Fig. 18 demonstrate another limitation of the deterministic prediction when multiple locations exceed the threshold. As shown in Fig. 17, the top and bottom panels of Fig. 18 show different node locations (i.e., Nodes 19 and 51) subjected to the same GM. The

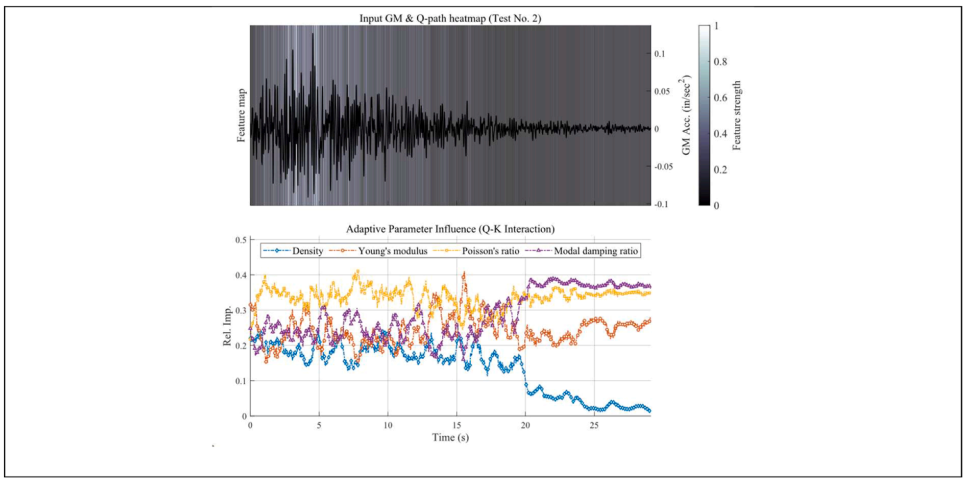

Fig. 16. Attention map visualization.

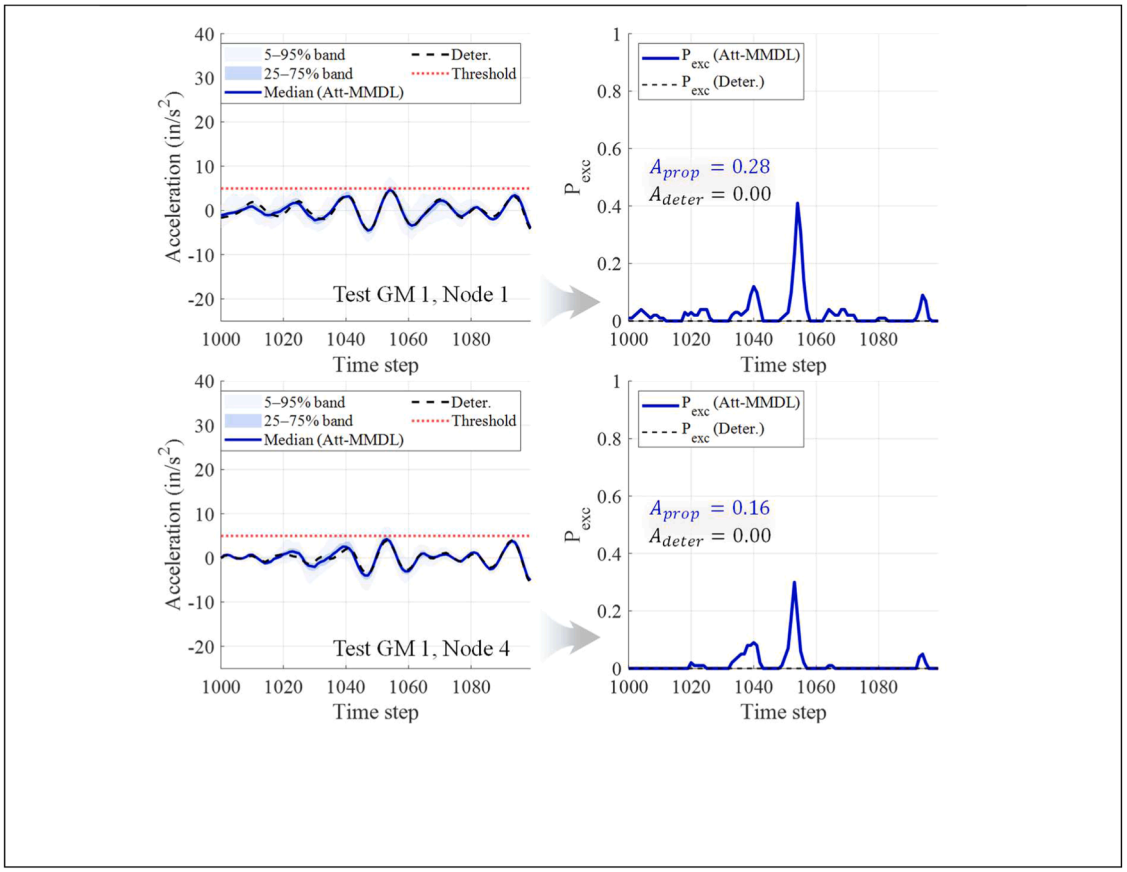

Fig. 17. Comparison of deterministic vs. probabilistic predictions. Left panels: acceleration time histories with uncertainty bands from 100 combinations of structural parameters ensembles. Red lines indicate safety threshold (i.e., 4.95 in/s^2). Right panels: P_{exc}(Att-MMDL) (i.e., blue) vs. P_{exc}(Deter.) (i.e., black dashed).

deterministic prediction indicated that both nodes had equal risk, providing no prioritization information between those nodes. A_{deter} for both nodes were identical at 0.8 because the deterministic prediction can only provide binary risk classification, where $P_{exc}(t)$ of each time step is counted as 1 if it exceeds the threshold or 0 otherwise. In contrast, the probabilistic prediction with the proposed model exhibited clearer risk quantification. For example, Node 51 (i.e., bottom panel) showed a higher A_{prop} of 1.16 than 0.58 for Node 34 (i.e., top panel). This substantial difference of 0.58 indicates that Node 51 posed a risk that was twice higher than that of Node 19, which provides useful information to guide decision-making in prioritizing that Node for inspection.

These results demonstrate that the probabilistic prediction leveraged by the proposed Att-MMDL framework can transform seismic risk assessment from binary classification into a process of continuous risk quantification. The ability to distinguish the risk of important equipment locations through temporal exceedance probabilities while accounting for structural parameter uncertainties represents a significant advancement in risk-informed decision-making for NPPs. This improvement is especially critical when deterministic predictions assign equal risk across locations. This enhanced capability of the proposed

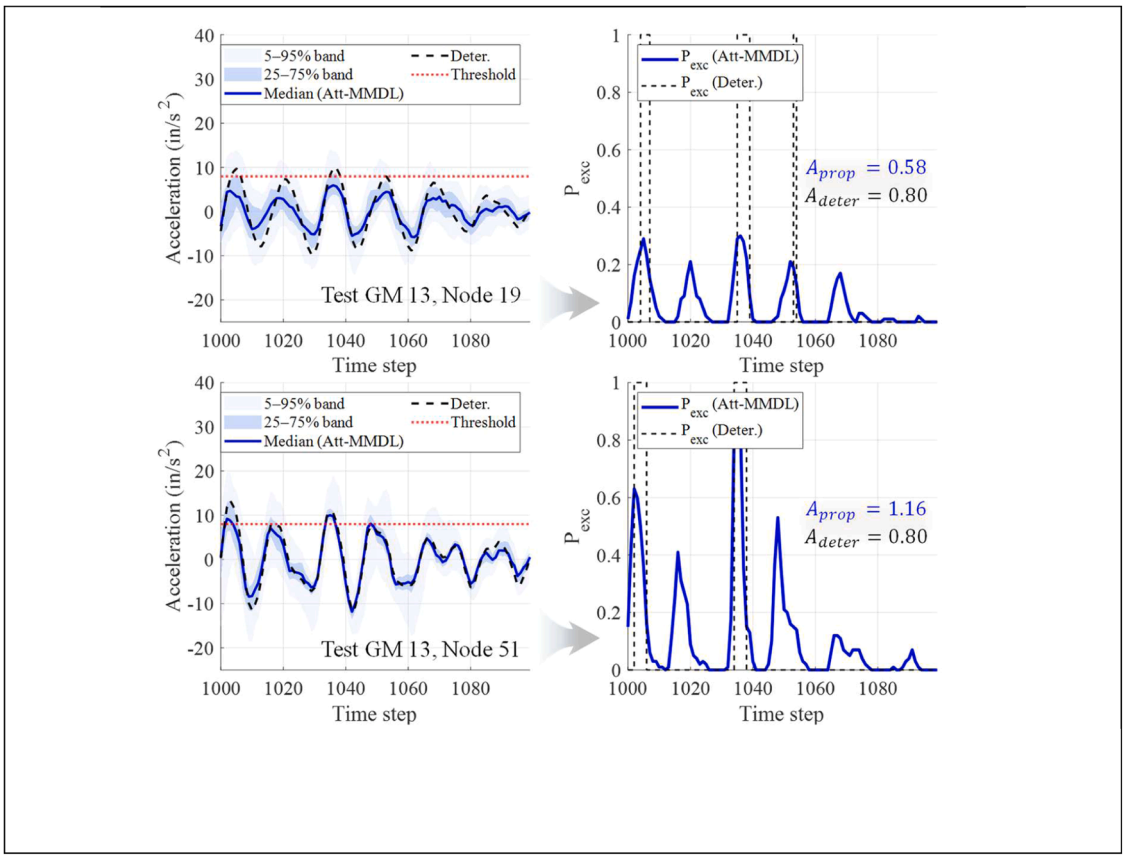

Fig. 18. Comparison of deterministic vs. probabilistic predictions. Left panels: acceleration time histories with uncertainty bands from 100 combinations of structural parameters ensembles. Red lines indicate safety threshold (i.e., 7.97 in/s^2). Right panels: P_{exc}(Att-MMDL) (i.e., blue) vs. P_{exc}(Deter.) (i.e., black dashed).

model is particularly valuable during seismic events when multiple important pieces of equipment may require simultaneous attention, because it can enable operators to prioritize inspections and allocate limited resources based on quantitative risk metrics rather than subjective judgment. Furthermore, continuous temporal exceedance probabilities facilitate the implementation of adaptive safety margins and risk-informed maintenance strategies. Rather than relying solely on deterministic thresholds, operators can incorporate uncertainty with respect to structural parameters into their decision-making criteria, which could improve both safety and operational efficiency by supporting more informed risk management practices.

5. Conclusion

In this study, we proposed the Att-MMDL framework for real-time seismic response prediction in NPP structures, introducing a cross-modal attention mechanism that enables seismic features to adaptively query and weight structural parameters as the GM evolves. This design captures time-varying parameter influences more effectively than conventional fusion approaches, thereby improving both representational capacity and physical consistency. The interpretability of the proposed model is further supported by attention visualization results, which demonstrate that the relative sensitivity of structural parameters varies in accordance with the GM acceleration over time. This behavior indicates that the framework learns time-varying relative importance across different phases of seismic excitation, rather than relying on fixed parameter weighting or black-box correlations.

Comprehensive evaluation against high-fidelity MC-based FE simulations verified the effectiveness and practical utility of the proposed model. The Att-MMDL model achieved high prediction accuracy with a relative error of 0.95 % while reducing inference time to the millisecond scale, confirming its suitability for rapid post-earthquake decision-making. Moreover, the predicted uncertainty bands closely matched the true response distributions, demonstrating reliable uncertainty propagation under variability in both GM and structural parameters. Importantly, the probabilistic nature of the framework enables continuous risk quantification beyond deterministic predictions, providing a more informative ranking of node-level risk even when deterministic assessments indicate identical zero-risk outcomes. This capability supports risk-informed prioritization of inspections and maintenance actions based on objective probability metrics.

Despite these promising results, this study has limitations that should be addressed in future research. The proposed framework is developed under the assumption of linear elastic structural behavior, where responses can be accurately represented through modal superposition; therefore, it is applicable to design-level and moderate seismic excitations relevant to rapid assessment of equipment-level responses but is not intended to capture strongly nonlinear structural behavior induced by severe GMs. Nevertheless, the Att-MMDL framework itself is not inherently restricted to linear simulations. With appropriate training datasets generated from nonlinear time-history analyses and by incorporating additional sources of uncertainty associated with material nonlinearity or damage-state indicators, the framework could be extended in future work to serve as an uncertainty-aware surrogate for nonlinear FEA within a Probabilistic Risk Assessment (PRA). Furthermore, although the trained model demonstrated sufficient accuracy under different GM efficient durations, further improvements are still needed to achieve more consistent and uniformly high accuracy across a broader range of durations and temporal characteristics. Overall, the proposed Att-MMDL model provides a scalable foundation for uncertainty-aware seismic response prediction by bridging the gap between high-fidelity simulation-based assessment and operational speed

requirements for NPP safety management.

CRediT authorship contribution statement

Jingoo Lee: Writing – original draft, Visualization, Validation, Methodology, Investigation, Formal analysis, Data curation, Conceptualization. **Seungjun Lee:** Writing – review & editing, Investigation, Conceptualization. **Young-Joo Lee:** Writing – review & editing, Supervision, Funding acquisition, Conceptualization. **Jaebeom Lee:** Writing – review & editing, Supervision, Funding acquisition, Conceptualization.

Declaration of competing interest

The authors declare that they have no known competing financial interests or personal relationships that could have appeared to influence the work reported in this paper.

Acknowledgements

This work was supported by the National Research Foundation of Korea (NRF) grant funded by the Korea government (MSIT) (No. RS-2022-00144434) and also supported by 'Developing digital safety measurement to enhance the availability of smart structural monitoring of facilities' funded by Korea Research Institute of Standards and Science (KRISS) (KRISS-2026-GP2026-0009).

Data availability

The data that support the findings of this study are confidential and therefore not publicly available. However, to support the reproducibility of this research, the implementation of the proposed model has been made publicly available at GitHub: https://github.com/jingoo-lee/Att-MMDL.

References

[1] Korea Hydro & Nuclear Power (KHNP). Measures taken in accordance with emergency manuals following overall check-ups of all power generation. September 13. KHNP Press Center; 2016. in Korean.
[2] Virginia Electric and Power Company (VEPC). 10 CFR 50.73 licensee event report. north anna power station, mineral, virginia. November 23. 2011. https://www.nrc.gov/docs/ML1134/ML11340A034.pdf.
[3] U.S. Nuclear Regulatory Commission (NRC). Technical evaluation by the office of nuclear reactor regulation: related to plant restart after the occurrence of an earthquake exceeding the level of the operating basis and design basis earthquakes (North anna power station, unit nos. 1 and 2; docket nos. 50-338 and 50-339). November 11. Washington, DC: U.S. NRC; 2011. https://www.nrc.gov/docs/ML1130/ML11308B406.pdf.
[4] Schlupp A, Sira C, Maufroy E, Provost L, Dretzen R, Bertrand E, Schaming M. EMS98 intensities distribution of the "Le Teil" earthquake, France, 11 November 2019 (Mw 4.9) based on macroseismic surveys and field investigations. C R Géosci 2021;353(S1):465–92. https://doi.org/10.5802/crgeos.88.
[5] Zheng Z, Zhang P, Pan X, Yang F. Deep Learning-Enhanced Multi-Fidelity Framework for seismic fragility analysis of nuclear power plant containment structures: submitted to: reliability engineering & System safety. Reliab Eng Syst Saf 2025:111884. https://doi.org/10.1016/j.ress.2025.111884.
[6] Der Kiureghian A, Ditlevsen O. Aleatory or epistemic? Does it matter? Struct saf 2009;31(2):105–12. https://doi.org/10.1016/j.strusafe.2008.06.020.
[7] Lavrentiadis G, Abrahamson NA, Nicolas KM, Bozorgnia Y, Goulet CA, Babič A, Walling M. Overview and introduction to development of non-ergodic earthquake ground-motion models. Bull Earthq Eng 2023;21(11):5121–50. https://doi.org/10.48550/arXiv.2111.07921.
[8] Zhao YG, Qin MJ, Lu ZH, Zhang LW. Seismic fragility analysis of nuclear power plants considering structural parameter uncertainty. Reliab Eng Syst Saf 2021;216:107970. https://doi.org/10.1016/j.ress.2021.107970.
[9] Dasgupta B. Evaluation of methods used to calculate seismic fragility curves (Contract No. NRC–HQ–12–C–02–0089). Center for nuclear waste regulatory analyses. San Antonio, TX: Prepared for the U.S. Nuclear Regulatory Commission; 2017. https://www.nrc.gov/docs/ML1712/ML17122A268.pdf.
[10] Ghanem RG, Spanos PD. Stochastic finite elements: a spectral approach. Courier Corporation; 2003.
[11] Sudret B. Global sensitivity analysis using polynomial chaos expansions. Reliabi Eng Syst Saf 2008;93(7):964–79. https://doi.org/10.1016/j.ress.2007.04.002.
[12] Pak H, Leach S, Yoon SH, Paal SG. A knowledge transfer enhanced ensemble approach to predict the shear capacity of reinforced concrete deep beams without stirrups. Comput-Aided Civ Infrastruct Eng 2023;38(11):1520–35. https://doi.org/10.1111/mice.12965.
[13] Kazemi F, Asgarkhani N, Jankowski R. Machine learning-based seismic fragility and seismic vulnerability assessment of reinforced concrete structures. Soil Dyn Earthq Eng 2023;166:107761. https://doi.org/10.1016/j.soildyn.2023.107761.
[14] Asgarkhani N, Kazemi F, Jakubczyk-Gałczyńska A, Mohebi B, Jankowski R. Seismic response and performance prediction of steel buckling-restrained braced frames using machine-learning methods. Eng Appl Artif Intell 2024;128:107388. https://doi.org/10.1016/j.engappai.2023.107388.
[15] Jia J, Gong M, Zuo Z, Wang X, Zhao Y. A novel deep learning-based method for generating floor response spectra of building structures. Eng Struct 2025;322:119058. https://doi.org/10.1016/j.engstruct.2024.119058.
[16] Zhong QM, Chen SZ, Feng DC. Multi-output time history prediction for seismic responses of structures with uncertain parameters via deep learning. In structures, 76. Elsevier; 2025, 108905. https://doi.org/10.1016/j.istruc.2025.108905.
[17] Jia J, Gong M, Zuo Z, Wang X, Zhao Y, Liu B. Generating elastic floor response spectra using ensemble learning methods with whale optimization algorithm. Structures, 82. Elsevier; 2025, 110587. https://doi.org/10.1016/j.istruc.2025.110587.
[18] Zhou Y, Meng S, Xu H, Chen J, Wu H. A real-time multi-node structural response prediction and rapid seismic resilience assessment method. Reliab Eng Syst Saf 2025;258:110889. https://doi.org/10.1016/j.ress.2025.110889.
[19] Lee J, Lee S, Lee YJ, Lee J. Virtual sensing of seismic floor responses for rapid prioritization of critical equipment inspection in nuclear power plants. Comput-Aided Civ Infrastruct Eng 2025. https://doi.org/10.1111/mice.70051.
[20] Karami R, Yazdanpanah O, Dolatshahi KM, Chang M. Hybrid stacked neural network empowered by novel loss function for structural response history prediction using input excitation and roof acceleration. Eng Appl Artif Intell 2024;136:108984. https://doi.org/10.1016/j.engappai.2024.108984.
[21] Jia J, Gong M, Zuo Z, Liu B. Real-time structural seismic time history response prediction based on physics-informed deep learning. J Build Eng 2025:112932. https://doi.org/10.1016/j.jobe.2025.112932.
[22] Pak H, Paal SG. A real-time structural seismic response prediction framework based on transfer learning and unsupervised learning. Eng Struct 2025;323:119227. https://doi.org/10.1016/j.engstruct.2024.119227.
[23] Vaswani A, Shazeer N, Parmar N, Uszkoreit J, Jones L, Gomez AN, Kaiser Ł, Polosukhin I. Attention is all you need. Advances in neural information processing systems, 30. Curran Associates, Inc; 2017. https://arxiv.org/abs/1706.03762.
[24] Shi P, Jia T, Xu X, Han D. A generative dual-input model based on architectural computational optimization and multi-attention mechanism for remaining useful life prediction. Reliab Eng Syst Saf 2025:111777. https://doi.org/10.1016/j.ress.2025.111777.
[25] Han J, Kwon Y, Yoon H. Mamba-attention: a self-supervised framework for efficient remaining useful life prediction. Reliab Eng Syst Saf 2025:111492. https://doi.org/10.1016/j.ress.2025.111492.
[26] Zhou L, Wang H, Xu S. An adaptive multi-scale spatial-temporal graph attention ensemble network with physical guidance for remaining useful life prediction of multi-sensor equipment. Reliab Eng Syst Saf 2025:111152. https://doi.org/10.1016/j.ress.2025.111152.
[27] Peng K, Zhou W, Jiang L, Xiong L, Yan WJ. Multimodal fusion hybrid neural network approach for multi-class damage classification in high-speed rail track-bridge systems with multi-parameter. Eng Struct 2025;328:119710. https://doi.org/10.1016/j.engstruct.2025.119710.
[28] Ngiam J, Khosla A, Kim M, Nam J, Lee H, Ng AY. Multimodal deep learning. In ICML 2011;11:689–96.
[29] Bouchey B, Castek J, Thygeson J. Multimodal learning. Innovative learning environments in stem higher education: opportunities, challenges, and looking forward. Cham: Springer International Publishing; 2021. p. 35–54.
[30] Ma Q, Kwon OS, Kwon TH, Choun YS. Influence of frequency content of ground motions on seismic fragility of equipment in nuclear power plant. Eng Struct 2020;224:111220. https://doi.org/10.1016/j.engstruct.2020.111220.
[31] Yoshitake I, Rajabipour F, Mimura Y, Scanlon A. A prediction method of tensile Young′ s modulus of concrete at early age. Adv Civ Eng 2012;2012(1):391214. https://doi.org/10.1155/2012/391214.
[32] Wang Z, Pedroni N, Zentner I, Zio E. Seismic fragility analysis with artificial neural networks: application to nuclear power plant equipment. Eng Struct 2018;162:213–25. https://doi.org/10.1016/j.engstruct.2018.02.024.
[33] Vu CC, Weiss J, Plé O, Amitrano D. The potential impact of size effects on compressive strength for the estimation of the Young's modulus of concrete. Mater struct 2021;54(5):196. https://doi.org/10.1617/s11527-021-01795-7.
[34] Li C, Mahadevan S. Relative contributions of aleatory and epistemic uncertainty sources in time series prediction. Int J Fatigue 2016;82:474–86. https://doi.org/10.1016/j.ijfatigue.2015.09.002.
[35] JCSS (Joint Committee on Structural Safety). Probabilistic model code. Part 3: resistance models. chrome-extension://efaidnbmnnnibpcajpcglclefindmkaj/, https://www.jcss-lc.org/publications/jcsspmc/part_iii.pdf; 2001.
[36] Ghahari F, Sargsyan K, Taciroglu E. Quantification of modeling uncertainty in the Rayleigh damping model. Earthq Eng Struct Dyn 2024;53(9):2950–6. https://doi.org/10.1002/eqe.4143.
[37] Hüllermeier E, Waegeman W. Aleatoric and epistemic uncertainty in machine learning: an introduction to concepts and methods. Mach Learn 2021;110(3):457–506. https://doi.org/10.1007/s10994-021-05946-3.

[38] Avendaño-Valencia LD, Chatzi EN, Koo KY, Brownjohn JM. Gaussian process time-series models for structures under operational variability. Front Built Environ 2017;3:69. https://doi.org/10.3389/fbuil.2017.00069.
[39] Hu Z, Mahadevan S, Ao D. Uncertainty aggregation and reduction in structure–material performance prediction. Comput Mech 2018;61(1):237–57. https://doi.org/10.1007/s00466-017-1448-6.
[40] Hinton GE, Salakhutdinov RR. Reducing the dimensionality of data with neural networks. science 2006;313(5786):504–7. https://doi.org/10.1126/science.1127647.
[41] Lee, J., Lee, Y.J., & Lee, Y.J. (2025). Design of 1D CNN kernels for predicting seismic response of nuclear power plants.
[42] Rezaeian S, Der Kiureghian A. Simulation of synthetic ground motions for specified earthquake and site characteristics. Earthq Eng Struct Dyn 2010;39(10):1155–80. https://doi.org/10.1002/eqe.997.
[43] Shin KH, Kim C, Nam SH, Park SJ, Yoo SS. Estimation method of predicted time series data based on absolute maximum value. J Energy Eng 2018;27(4):103–10. https://doi.org/10.5855/ENERGY.2018.27.4.103.